# Electromagnetic Imaging for an Imperfectly Conducting Cylinder

Chien-Ching Chiu and Yean-Woei Kiang, *Member, IEEE*

*Abstract*—**This paper presents a computational approach to the imaging or inverse scattering of an imperfectly conducting cylinder. A conducting cylinder of unknown shape and conductivity scatters the incident wave in free space and the scattered field is recorded on a circle surrounding the scatterer. By properly processing the scattered data, the shape and conductivity of the scatterer can be reconstructed. The problem is formulated in the form of nonlinear integral equations which can be solved numerically by the Newton–Kantorovitch algorithm. The pseudoinverse technique is used to overcome the ill-posedness, and the condition number of the matrix is also discussed. Numerical examples are given to illustrate the capability of the inversion algorithm using the simulated scattered fields in both near and far zones. Multiple incident directions permit good reconstruction of shape and, to a lesser extent, conductivity in the presence of noise in measured data.**

## I. Introduction

THE electromagnetic inverse scattering problem has attracted increasing attention owing to interests in noninvasive measurement and remote sensing. The development of practical numerical techniques for the inverse scattering problem is important and urgent. However, inverse problems of this type are difficult to solve because they are both ill posed and nonlinear. In the past few years, several numerical techniques have been reported for inverse scattering problems. Generally speaking, two kinds of approaches have been developed. The first is an approximate approach. It makes use of a diffraction tomography type of technique to determine the permittivity of a dielectric object [1], [2] or employs the Bojarski identity to recover the shape of a perfectly conducting scatterer [3], [4]. However, this method requires some approximations, such as the Born approximation for dielectric objects and a physical optics approximation for perfectly conducting scatterers. In contrast, the second approach is to solve the exact equation of the inverse scattering problem by numerical methods [5]–[10]. This technique needs no approximation in formulation, but the calculation is more complex than the approximate approach stated above. However, for metallic scatterers, the aforementioned methods merely dealt with the case of perfectly conducting objects, and there is still no rigorous algorithm for the case involving lossy or imperfect metallic scatterers.

Inverse problems usually reveal numerical instability: small noise contaminating the data may produce fairly large error in the solution. In other words, these problems are ill posed. To overcome the ill-posedness, several numerical techniques have been reported, such as the singular value decomposition method [9], [10], the pseudoinverse transformation [5], [11], and the penalized likelihood method [8]. From a mathematical viewpoint, the singular value decomposition method and the pseudoinverse transformation are equivalent. Although the penalized likelihood method seems different from the other two methods, in many cases they lead to similar effects in circumventing the ill-posedness.

In this paper, the inverse scattering from an imperfectly conducting (i.e., lossy) cylinder in free space is investigated. We propose an algorithm to recover not only the shape but also the conductivity of a scatterer, by using only the scattered field. This algorithm is based on the Newton–Kantorovitch method. In Section II, the theoretical formulation for the inverse scattering is presented. We then introduce numerical techniques to solve the integral equations and to overcome the ill-posedness, in Section III. Numerical results for objects of different shapes and conductivities are given in Section IV. Finally, some conclusions are drawn in Section V.

## II. Theoretical Formulation

Let us consider an imperfectly conducting cylinder with conductivity $\sigma$ located in free space and let $(\epsilon_0, \mu_0)$ denote the permittivity and permeability respectively of free space. The metallic cylinder with cross section described in polar coordinates in the $xy$ plane by the equation $\rho = F(\theta)$ is illuminated by an incident plane wave whose electric field vector is parallel to the $z$ axis (i.e., transverse magnetic, or TM, polarization). We assume that the time dependence of the field is harmonic with the factor $\exp(j\omega t)$. Let $\vec{E}_i$ denote the incident field with incident angle $\phi$, as shown in Fig. 1. Then the incident field is given by

$$\vec{E}_i(\vec{r}) = e^{-jk(x\sin\phi + y\cos\phi)}\hat{z} \qquad k^2 = \omega^2\epsilon_0\mu_0. \tag{1}$$

At an arbitrary point $(x, y)$ in Cartesian coordinates or

Manuscript received January 9, 1991; revised April 15, 1991. This work was supported by the National Science Council, Republic of China, under Grant NSC 79-0404-E002-22.

The authors are with the Department of Electrical Engineering, National Taiwan University, Taipei, Taiwan, Republic of China.

IEEE Log Number 9101651.

0018-9480/91/0900-1632$01.00 ©1991 IEEE

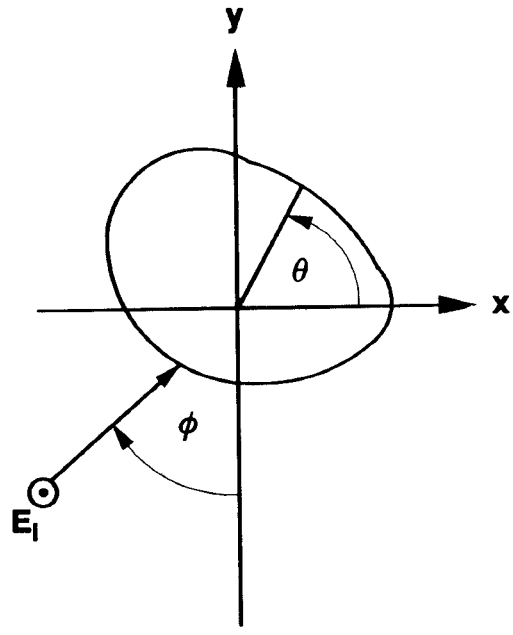


Fig. 1. Geometry of the problem in the $(x, y)$ plane.

$(r,\theta)$ in polar coordinates outside the scatterer, the scattered field, $\vec{E}_s = \vec{E} - \vec{E}_i$, can be expressed by

$$E_s(x,y) = -\int_0^{2\pi} \frac{j}{4} H_0^{(2)} \cdot \left(k\sqrt{(x - F(\theta')\cos(\theta'))^2 + (y - F(\theta')\sin(\theta'))^2}\right) J(\theta')\, d\theta' \tag{2}$$

with

$$J(\theta) = -j\omega\mu_0 \sqrt{F^2(\theta) + F'^2(\theta)}\, J_s(\theta)$$

where $H_0^{(2)}$ is the Hankel function of the second kind of order zero, and $J_s(\theta)$ is the induced surface current density, which is proportional to the normal derivative of the electric field on the conductor surface. Note that the scattered field for large values of $r$ in (2) can be expressed in asymptotic form as

$$E_s(x,y) \sim \frac{e^{-jkr}}{\sqrt{r}} G_s(\theta)$$

$$G_s(\theta) = -\frac{j}{4}\sqrt{\frac{2}{\pi k}}\, e^{j\pi/4} \int_0^{2\pi} e^{jkF(\theta')\cos(\theta - \theta')} J(\theta')\, d\theta' \tag{2}'$$

where $G_s(\theta)$ is known as the scattered far-field pattern.

For an imperfectly conducting scatterer with finite conductivity, the electromagnetic wave is able to penetrate into the interior of a scatterer, so the total tangential electric field at the surface of the scatterer is not equal to zero. As described in [12] and [13], the boundary condition for this case can be approximated by assuming that the total tangential electric field on the scatterer surface is related to the surface current density through a surface impedance $Z_s(\omega)$:

$$\hat{n} \times \vec{E} = \hat{n} \times \left(Z_s \vec{J}_s\right). \tag{3}$$

where $\hat{n}$ is the outward unit vector normal to the surface of the scatterer. The scatterer of interest here is a nonmagnetic ($\mu = \mu_0$), imperfectly conducting cylinder with minimum radius of curvature $a$. The surface impedance is expressed in [12] and [13] as $Z_s(\omega) \simeq \sqrt{j\omega\mu_0/\sigma}$. This approximation is valid as long as $|\mathrm{Im}(N_c)ka| \gg 1$ and $\sigma \gg \omega\epsilon_0$, where "Im" means taking the imaginary part, and $N_c$ is the complex index of refraction of the conductor, given by $N_c = \sqrt{1 + \frac{\sigma}{j\omega\epsilon_0}}$. The boundary condition at the surface of the scatterer given by (3) then yields an integral equation for $J(\theta)$:

$$E_i(F(\theta),\theta) = \int_0^{2\pi} \frac{j}{4} H_0^{(2)}(kr_0) J(\theta')\, d\theta' + j\sqrt{\frac{j}{\omega\mu_0\sigma}}\, \frac{J(\theta)}{\sqrt{F^2(\theta) + F'^2(\theta)}} \tag{4}$$

where

$$r_0(\theta,\theta') = \left[F^2(\theta) + F^2(\theta') - 2F(\theta)F(\theta')\cos(\theta - \theta')\right]^{\frac{1}{2}}.$$

For the direct scattering problem, the scattered field, $E_s$, is calculated by assuming that the shape and the conductivity of the object are known. This can be achieved by first solving $J$ in (4) and calculating $E_s$ in (2).

Next, we consider the following inverse problem: given the scattered field, $E_s$, measured outside the scatterer, determine the shape, $F(\theta)$, and conductivity, $\sigma$, of the object. Since (2) is a Fredholm integral equation of the first kind, the inverse problem of this type is ill posed. Furthermore, this problem is complicated because of the nonlinear dependence of (2) and (4) on $F(\theta)$ and $\sigma$. In our inverse method, the Newton–Kantorovitch algorithm is used to solve the nonlinear integral equations (2) and (4), and the pseudoinverse technique is employed to overcome the ill-posedness.

First, we define the nonlinear functional systems as

$$h(F,\sigma,J) = E_i(F(\theta),\theta) - \int_0^{2\pi} \frac{j}{4} H_0^{(2)}(kr_0) J(\theta')\, d\theta' - j\sqrt{\frac{j}{\omega\mu_0\sigma}}\, \frac{J(\theta)}{\sqrt{F^2(\theta) + F'^2(\theta)}} \tag{5}$$

$$f(F,\sigma,J) = E_s(x,y) + \int_0^{2\pi} \frac{j}{4} H_0^{(2)}\left(k\sqrt{(x - F(\theta')\cos(\theta'))^2 + (y - F(\theta')\sin(\theta'))^2}\right) \cdot J(\theta')\, d\theta' \tag{6}$$

and let the symbols $\delta h$ and $\delta f$ denote small variations of the quantities $h$ and $f$, respectively, caused by small

variations in $\delta F$, $\delta\sigma$, and $\delta J$. By differentiating (5) and (6), one obtains

$$\delta h(F,\sigma,J) = (-jk)(\cos\theta\sin\phi+\sin\theta\cos\phi)E_t(F(\theta),\theta)\,\delta F(\theta) - \int_0^{2\pi}\delta\left[\frac{j}{4}H_0^{(2)}(kr_0)\right]J(\theta')\,d\theta'$$

$$-\int_0^{2\pi}\frac{j}{4}H_0^{(2)}(kr_0)\,\delta J(\theta')\,d\theta' - j\sqrt{\frac{j}{\omega\mu_0\sigma}}\,\frac{\delta J(\theta)}{\sqrt{F^2(\theta)+F'^2(\theta)}} + \frac{j}{2}\sqrt{\frac{j}{\omega\mu_0\sigma}}\,\frac{1}{\sigma}\,\frac{J(\theta)}{\sqrt{F^2(\theta)+F'^2(\theta)}}\,\delta\sigma$$

$$+ j\sqrt{\frac{j}{\omega\mu_0\sigma}}\,\frac{J(\theta)}{\left(\sqrt{F^2(\theta)+F'^2(\theta)}\right)^3}\left[F(\theta)\delta F(\theta)+F'(\theta)\,\delta F'(\theta)\right] \tag{7}$$

$$\delta f(F,\sigma,J) = \int_0^{2\pi}\delta\left\{\frac{j}{4}H_0^{(2)}\left(k\sqrt{(x-F(\theta')\cos(\theta'))^2+(y-F(\theta')\sin(\theta'))^2}\right)\right\}J(\theta')\,d\theta'$$

$$+\int_0^{2\pi}\frac{j}{4}H_0^{(2)}\left(k\sqrt{(x-F(\theta')\cos(\theta'))^2+(y-F(\theta')\sin(\theta'))^2}\right)\delta J(\theta')\,d\theta' \tag{8}$$

where

$$\delta\left[\frac{j}{4}H_0^{(2)}(kr_0)\right] = \frac{-jk}{4}\left[\frac{F(\theta)-F(\theta')\cos(\theta-\theta')}{r_0}\,\delta F(\theta)+\frac{F(\theta')-F(\theta)\cos(\theta-\theta')}{r_0}\,\delta F(\theta')\right]H_1^{(2)}(kr_0)$$

$$\delta\left\{\frac{j}{4}H_0^{(2)}\left(k\sqrt{(x-F(\theta')\cos(\theta'))^2+(y-F(\theta')\sin(\theta'))^2}\right)\right\}$$

$$=\frac{-jk}{4}\left(\frac{F(\theta')-(x\cos\theta'+y\sin\theta')}{\sqrt{(x-F(\theta')\cos(\theta'))^2+(y-F(\theta')\sin(\theta'))^2}}\,\delta F(\theta')\right)$$

$$\cdot H_1^{(2)}\left(k\sqrt{(x-F(\theta')\cos(\theta'))^2+(y-F(\theta')\sin(\theta'))^2}\right).$$

To satisfy the boundary condition, $\delta h$ is set to zero. By using the least-squares method to solve (7) and (8), one obtains the differential increments of the shape function and the conductivity in each iteration. Then we can solve this inverse problem accordingly by an iterative procedure.

## III. Computational Technique

For numerical calculation of the direct problem, we use the moment method [14] to solve (4) and (2) with pulse basis functions $\{P_n(\theta)\}$ for expanding and Dirac delta functions for testing. Let

$$J(\theta) \simeq \sum_{n=1}^{M_d} B_n P_n(\theta).$$

Then (4) can be transformed into a matrix equation:

$$E_t(F(\theta_m),\theta_m) = \sum_{n=1}^{M_d} L_{mn}B_n \tag{9}$$

where

$$L_{mn} = \int_{\Delta C_n}\frac{j}{4}H_0^{(2)}(kr_0(\theta_m,\theta'))\,d\theta' + j\sqrt{\frac{j}{\omega\mu_0\sigma}}\,\frac{\delta_{mn}}{\sqrt{F^2(\theta_m)+F'^2(\theta_m)}}$$

and $\Delta C_i$ is the $i$th segment of the scatterer contour from $\theta = 2\pi(i-1)/M_d$ to $\theta = 2\pi i/M_d$. Note that the regularization procedure is hidden in the truncation of the series expansion of $J$. Also (2) becomes

$$E_s(\vec{r}) = -\sum_{n=1}^{M_d} B_n\int_{\Delta C_n}\frac{j}{4}H_0^{(2)}\cdot\left(k\sqrt{(x-F(\theta')\cos(\theta'))^2+(y-F(\theta')\sin(\theta'))^2}\right)d\theta'. \tag{10}$$

To solve (7) and (8) for the inverse problem, we choose the following expansions:

$$F(\theta) \simeq \sum_{n=0}^{\frac{N}{2}} A_n \cos(n\theta) + \sum_{n=1}^{\frac{N}{2}} A'_n \sin(n\theta)$$

$$J(\theta) \simeq \sum_{n=1}^{M} B_n P_n(\theta)$$

where $A_n$ and $A'_n$ are real numbers, and $B_n$ are complex in general. Note that $M$ must be different from $M_d$ since it is crucial that the synthetic data generated through a forward solver not be like those obtained by the inverse solver. In general, $M_d$ is chosen to be $2M$ in our calculation. For convenience, a vector $\vec{F}$ is defined by

$$(\vec{F})_i = \begin{cases} A_i, & 0 \leqslant i \leqslant N/2 \\ A'_{i-N/2}, & N/2+1 \leqslant i \leqslant N \\ \sigma, & i = N+1. \end{cases}$$

By the point matching technique, (7) and (8) can be cast into matrix form as

$$\delta\vec{h} = \hat{S}' \cdot \delta\vec{F} + \hat{U} \cdot \delta\vec{B} \tag{11}$$

$$\delta\vec{f} = \hat{C}' \cdot \delta\vec{F} + \hat{T} \cdot \delta\vec{B} \tag{12}$$

where

$$(\delta\vec{F})_i = \begin{cases} \delta A_i, & 0 \leqslant i \leqslant N/2 \\ \delta A'_{i-N/2}, & N/2+1 \leqslant i \leqslant N \\ \delta\sigma, & i = N+1 \end{cases}$$

$$(\delta\vec{B})_i = \delta B_i \qquad 1 \leqslant i \leqslant M$$

$$(\hat{S}')_{ij} = \begin{cases} S_{ij}, & 1 \leqslant i \leqslant M,\ 0 \leqslant j \leqslant N/2 \\ S'_{ij-N/2}, & 1 \leqslant i \leqslant M,\ N/2+1 \leqslant j \leqslant N \\ H_i, & 1 \leqslant i \leqslant M,\ j = N+1 \end{cases}$$

$$(\hat{U})_{ij} = U_{ij}, \qquad 1 \leqslant i \leqslant M,\ 1 \leqslant j \leqslant M$$

$$(\hat{C}')_{ij} = \begin{cases} C_{ij}, & 1 \leqslant i \leqslant M',\ 0 \leqslant j \leqslant N/2 \\ C'_{ij-N/2}, & 1 \leqslant i \leqslant M',\ N/2+1 \leqslant j \leqslant N \\ 0, & 1 \leqslant i \leqslant M',\ j = N+1 \end{cases}$$

$$(\hat{T})_{ij} = T_{ij}, \qquad 1 \leqslant i \leqslant M',\ 1 \leqslant j \leqslant M$$

where $M'$ is the number of measurement points. $S_{mn}$, $S'_{mn}$, $H_m$, $U_{mn}$, $C_{mn}$, $C'_{mn}$, and $T_{mn}$ are appropriate coefficients that can be obtained by tedious mathematical manipulations (see the Appendix).

To satisfy the boundary condition, we set $\delta\vec{h} = 0$. After eliminating $\delta\vec{B}$ in (12), we get

$$\delta\vec{f} = \left(\hat{C}' - \hat{T} \cdot \hat{U}^{-1} \cdot \hat{S}'\right) \cdot \delta\vec{F} \triangleq \hat{D} \cdot \delta\vec{F}.$$

By using the least-squares method and the Newton–Kantorovitch technique, one obtains the differential increment $\delta\vec{F}$ in each iteration:

$$\delta\vec{F} = -\left[\mathrm{Re}\,\hat{D}^{\dagger} \cdot \hat{D}\right]^{-1} \cdot \mathrm{Re}\left[\hat{D}^{\dagger} \cdot \vec{f}\right] \tag{13}$$

where the dagger (†) denotes transpose and complex conjugate, and "Re" means taking the real part. Since elements of $\delta\vec{F}$ are real quantities, we take the real parts of $\hat{D}^{\dagger} \cdot \hat{D}$ and $\hat{D}^{\dagger} \cdot \vec{f}$. Note that (13) is effective only for a single incoming wave. To overcome the difficulty of ill-posedness, we generalize the equation to the case of incoming waves of multi-incident angles by using the following formula:

$$\begin{aligned} \delta\vec{F} &= -\left[\mathrm{Re}\left(\hat{D}_1^{\dagger} \cdot \hat{D}_1 + \hat{D}_2^{\dagger} \cdot \hat{D}_2 + \cdots\right)\right]^{-1} \\ &\quad \cdot \mathrm{Re}\left[\hat{D}_1^{\dagger} \cdot \vec{f}_1 + \hat{D}_2^{\dagger} \cdot \vec{f}_2 + \cdots\right] \\ &\triangleq -\left[\mathrm{Re}\left(\hat{D}_i^{\dagger} \cdot \hat{D}_i\right)\right]^{-1} \cdot \mathrm{Re}\left[\hat{Q}_i\right] \end{aligned} \tag{14}$$

where $\hat{D}_i$ and $\vec{f}_i$ correspond to the $i$th incoming wave.

Although $\mathrm{Re}(\hat{D}_i^{\dagger} \cdot \hat{D}_i)$ is a real, symmetric square matrix, it is very difficult to ascertain whether the matrix $\mathrm{Re}(\hat{D}_i^{\dagger} \cdot \hat{D}_i)$ is invertible. Even when some care is taken to select the locations of observation points, the matrix $\mathrm{Re}(\hat{D}_i^{\dagger} \cdot \hat{D}_i)$ still may be numerically singular, and a solution of (14) is impractical. Therefore, regularization is needed. Rather than finding a solution by directly solving (14), an alternative approach is to find an estimated solution such that

$$\left\| \mathrm{Re}\left[\hat{D}_i^{\dagger} \cdot \hat{D}_i\right] \delta\vec{F} + \mathrm{Re}\left[\hat{Q}_i\right] \right\| \tag{15a}$$

is minimum with the condition

$$\|\delta\vec{F}\| \text{ is minimum} \tag{15b}$$

where $\|\cdot\|$ denotes the norm. Equation (15) is then solved by means of a pseudoinverse algorithm [11] which is based on the Gram–Schmidt orthogonalization. The pseudoinverse transformation circumvents numerical instability inherent in inverse scattering and generates a unique solution for (15). The minimization of $\|\delta\vec{F}\|$ can to a certain extent be interpreted as the smoothness requirement for the boundary of $F(\theta)$. Therefore, the condition of (15) is minimization of the least-squares error between the measured field and the calculated field with the constraint of a smooth boundary. In reality, the matrix $\mathrm{Re}(\hat{D}_i^{\dagger} \cdot \hat{D}_i)$ is not absolutely singular. However, in order to find the pseudoinverse solution of (15), one has to set some of its column vectors as linearly dependent. In our calculation, the number of dependent columns is chosen so as to minimize the difference between the measured field and the calculated field in the least-squares sense in each iteration.

During the implementation of the iterative procedure, we first choose the initial guess $(\vec{F})^0$ and solve for $(\delta\vec{F})^k$ in (15) to obtain $(\vec{F})^{k+1} = (\vec{F})^k + (\delta\vec{F})^k$, $k = 0, 1, 2, 3 \cdots$. Iteration continues until convergence is achieved. To monitor convergence, after each iteration the calculated profile, $F^{\mathrm{cal}}(\theta)$, and conductivity, $\sigma$, are substituted into (4) and (2) to produce the calculated scattered field,

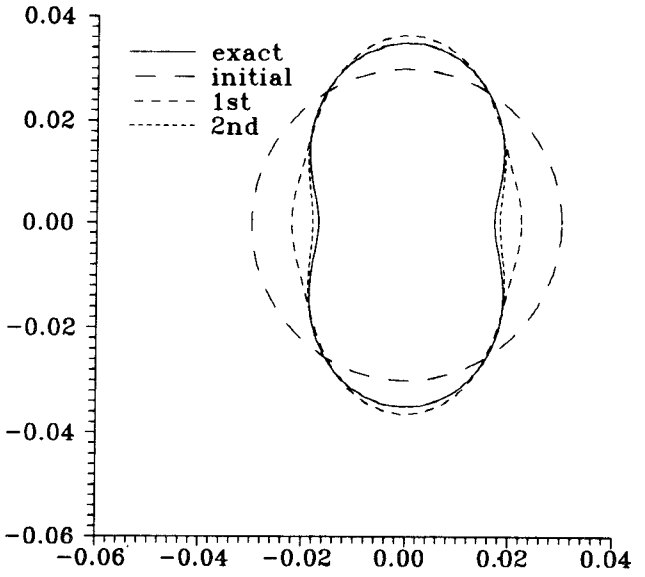


Fig. 2. Target profiles for example 1. The solid curve represents the exact profile, while the dashed curves are calculated profiles in iteration process.

$E_s^{\text{cal}}(\vec{r})$, and the discrepancy

$$\text{DF} = \left\{ \frac{1}{M_t'} \sum_{m=1}^{M_t'} \left| E_s^{\text{exp}}(\vec{r}_m) - E_s^{\text{cal}}(\vec{r}_m) \right|^2 / \left| E_s^{\text{exp}}(\vec{r}_m) \right|^2 \right\}^{1/2}$$

is determined, where $M_t'$ is the total number of measurement points and $E_s^{\text{exp}}$ the measured scattered field. Iteration will be stopped when either DF changes by less than 2% in two successive iterations or DF is smaller than $10^{-5}$ in two successive iterations.

## IV. Numerical Results

By a numerical simulation we illustrate the performance of the proposed inversion algorithm and its sensitivity to random error in the scattered field. Let us consider an imperfectly conducting cylinder in free space and a plane wave of unit amplitude incident upon the object, as shown in Fig. 1. The frequency of the incident wave is chosen to be 3 GHz; i.e., the wavelength $\lambda$ is 0.1 m. In the examples the size of the scatterer is about one third the wavelength, so the frequency is in the resonance range.

In our calculation three examples are considered. To reconstruct the shape and conductivity of the cylinder, the object is illuminated by four incident waves with incident angles $\phi = 0°, 90°, 180°$, and $270°$, and the measurement is taken on a circle of radius $R'$ at equal spacing. In our cases, $R'$ is chosen either much larger than or smaller than $2D'^2/\lambda$, corresponding to the far-field or near-field measurement respectively, where $D'$ is the largest dimension of the scatterer. Note that for each incident angle eight measurement points at equal spacing are used, and there are a total of 32 measurement points in each simulation. The number of unknowns is set to 10 (i.e., $N+2=10$) and $M$ is set to 100.

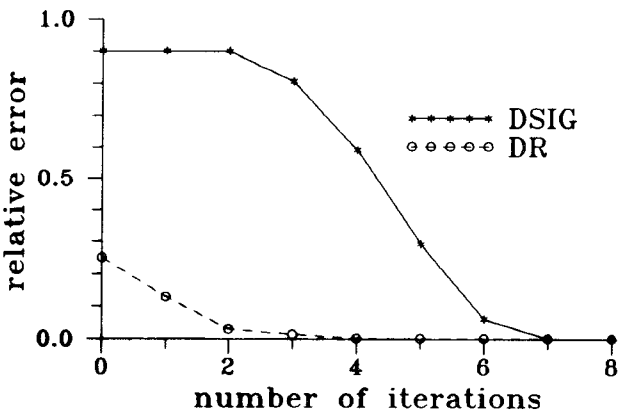


Fig. 3. Profile discrepancy (DR) and conductivity error (DSIG) in iteration process for example 1.

TABLE I
Condition Number of Matrix $\text{Re}(\hat{D}_t^{\dagger} \cdot \hat{D}_t)$ Before and After Regularization

| Number of Iterations | Condition Number Before Regularization | Condition Number After Regularization |
|---|---|---|
| 0 | 30987 | 8 |
| 1 | 30018 | 16 |
| 2 | 29153 | 29153 |
| 3 | 28850 | 28850 |
| 4 | 28828 | 28828 |
| 5 | 28823 | 28823 |
| 6 | 28821 | 28821 |
| 7 | 28820 | 8 |

We now report on three different shape functions and conductivities we have computed. Note that the reconstructed result of the last iteration in each example is not plotted since it cannot be distinguished from the exact one by the naked eye.

In the first example, the shape function is chosen to be $F(\theta) = (0.026 - 0.009\cos 2\theta)$ m with bronze material (i.e., $\sigma = 1.0 \times 10^7$ S/m). From the far-field measurement simulation, the reconstructed shape function is plotted in Fig. 2 with the error shown in Fig. 3, while the error for the reconstructed conductivity is also given in Fig. 3. Here DR and DSIG, which are called profile and conductivity discrepancies respectively, are defined as

$$\text{DR} = \left\{ \frac{1}{N'} \sum_{t=1}^{N'} \left[ F^{\text{cal}}(\theta_t) - F(\theta_t) \right]^2 / F^2(\theta_t) \right\}^{1/2}$$

$$\text{DSIG} = \left| \frac{\sigma^{\text{cal}} - \sigma}{\sigma} \right|$$

where $N'$ is set to 60. The quantities DR and DSIG provide measures of how well $F^{\text{cal}}$ approximates $F(\theta)$ and $\sigma^{\text{cal}}$ approximates $\sigma$ respectively. The measurement radius, $R'$, in this case is 7 m. From Fig. 3, it is clear that the reconstruction of the shape function and conductivity is quite good. The quantity DSIG is $1 \times 10^{-2}$ in the final iteration. In addition, we also see that the reconstruction of conductivity does not change rapidly toward the exact value until DR is small enough. This can be explained by the fact that the shape function makes a stronger contri-

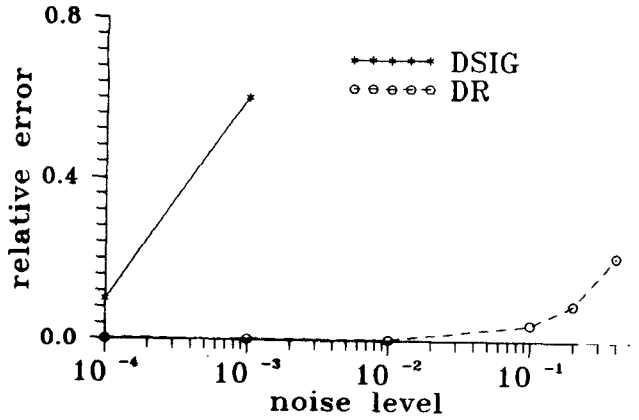


Fig. 4. Profile discrepancy (DR) and conductivity error (DSIG) for example 1 as functions of noise level.

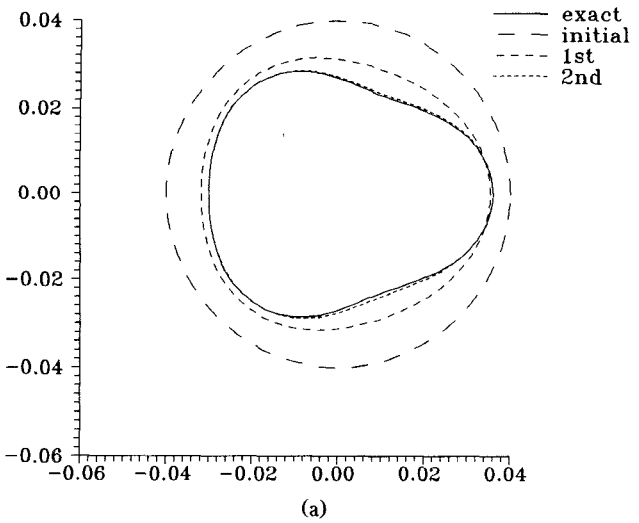


Fig. 5. Reconstructed results for example 2. (a) The solid curve represents the exact profile, while the dashed curves are calculated profiles in iteration process. (b) Profile discrepancy (DR) and conductivity error (DSIG) in iteration process.

bution to the scattered field than the conductivity does. In other words, the reconstruction of the shape function has a higher priority than the reconstruction of the conductivity.

The corresponding condition number of the matrix $\mathrm{Re}(\hat{D}_t^{\dagger}\cdot\hat{D}_t)$ in each iteration is listed in Table I. Listed in

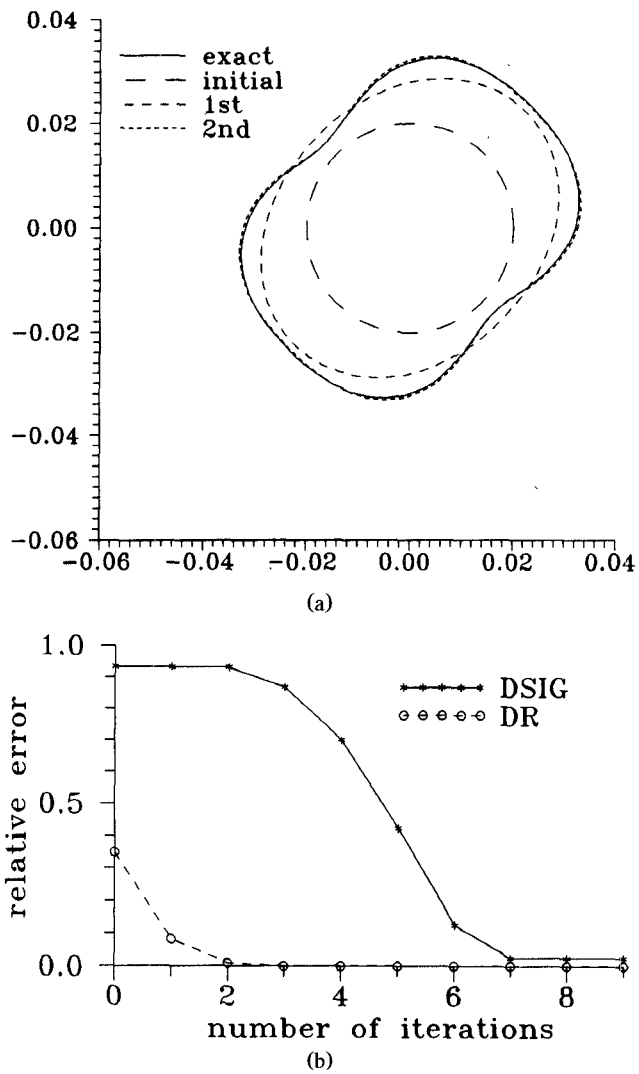


Fig. 6. Reconstructed results for example 3. (a) The solid curve represents the exact profile, while the dashed curves are calculated profiles in iteration process. (b) Profile discrepancy (DR) and conductivity error (DSIG) in iteration process.

the second column are the condition numbers before regularization (i.e., before using pseudoinverse transformation), while in the third column are those after regularization. From this table and Fig. 3, we can see that the DSIG varies considerably between the $i$th and $(i+1)$th iterations only when the condition number does not change after using the pseudoinverse transformation in the $i$th iteration. This is due to the fact that the adjustment of the conductivity during iteration is determined by the smallest eigenvalue of the matrix $\mathrm{Re}(\hat{D}_t^{\dagger}\cdot\hat{D}_t)$. In other words, as the pseudoinverse transformation sets the smallest eigenvalue of the matrix $\mathrm{Re}(\hat{D}_t^{\dagger}\cdot\hat{D}_t)$ to zero, i.e., the condition number is changed, the conductivity of the object will not be altered.

For investigating the effect of noise, we add to each complex scattered field $E_s(\vec{r})$ a quantity $b+cj$, where $b$ and $c$ are independent random numbers having a uniform distribution over 0 to the noise level times the R.M.S. value of scattered field. The noise levels applied include

$10^{-4}$, $10^{-3}$, $10^{-2}$, $10^{-1}$, $2\times10^{-1}$, and $4\times10^{-1}$. The numerical results are shown in Fig. 4. Since DSIG is too large at high noise level, it is not plotted at a noise level greater than $10^{-3}$ in this figure. This shows that the effect of noise is tolerable for noise levels below $10^{-4}$.

Next, we reconstruct the object by using scattered fields in the near zone. All parameters are the same as those in the far-field measurement, except that the measurement radius, $R'$, is chosen as 0.06 m. The quantity DSIG is $2\times10^{-3}$ in the final iteration. It is clear that the reconstructed results are better than those obtained by using far-field data.

In the second example, the shape function is chosen as $F(\theta)=(0.03+0.003\cos 2\theta+0.003\cos 3\theta)$ m, whereas aluminum material is selected (i.e., $\sigma=3.54\times10^{7}$ S/m). $R'$ is chosen as 7 m. The purpose of this example is to show that our method is able to reconstruct a scatterer whose shape function is not symmetrical about the $y$ axis. Satisfactory results are shown in Fig. 5.

In the third example, the shape function is selected to be $F(\theta)=(0.03+0.002\cos 4\theta+0.005\sin 2\theta)$ m with brass material (i.e., $\sigma=1.57\times10^{7}$ S/m), and $R'$ is chosen as 7 m. Note that the shape function is not symmetrical about either the $x$ axis or the $y$ axis. This example has further verified the reliability of our algorithm. Refer to Fig. 6 for details.

From the above three examples, we can conclude that our imaging or inverse scattering algorithm is accurate and can be implemented numerically.

## V. Conclusions

We have proposed an algorithm for reconstructing the shape and conductivity of a metallic object through knowledge of scattered field. The Newton–Kantorovitch algorithm and the moment method have been used to transform the nonlinear integral equations into matrix form. Then these matrix equations are solved by the pseudoinverse transformation to obtain a stable approximate solution. By means of the above numerical techniques, good reconstruction is obtained from the scattered field both with and without additive random noise. Several examples have illustrated that the inversion algorithm gives accurate reconstruction from measured data simulated numerically in near and far zones. Numerical results also illustrate that the conductivity is more sensitive to noise than the shape function is.

## Appendix

Given in the following are the matrix elements in (11) and (12):

$$S_{mn}=(-jk)(\cos\theta_m\sin\phi+\sin\theta_m\cos\phi)E_i(F(\theta_m),\theta_m)\cos(n\theta_m)$$

$$+\text{P.V.}\int_0^{2\pi}\frac{jk}{4}\frac{F(\theta_m)-F(\theta')\cos(\theta_m-\theta')}{r_0(\theta_m,\theta')}H_1^{(2)}(kr_0(\theta_m,\theta'))\cos(n\theta_m)J(\theta')\,d\theta'$$

$$+\text{P.V.}\int_0^{2\pi}\frac{jk}{4}\frac{F(\theta')-F(\theta_m)\cos(\theta_m-\theta')}{r_0(\theta_m,\theta')}H_1^{(2)}(kr_0(\theta_m,\theta'))\cos(n\theta')J(\theta')\,d\theta'$$

$$+j\sqrt{\frac{j}{\omega\mu_0\sigma}}\frac{J(\theta_m)}{\left(\sqrt{F^2(\theta_m)+F'^2(\theta_m)}\right)^3}[F(\theta_m)\cos(n\theta_m)-F'(\theta_m)n\sin(n\theta_m)]$$

$$S'_{mn}=(-jk)(\cos\theta_m\sin\phi+\sin\theta_m\cos\phi)E_i(F(\theta_m),\theta_m)\sin(n\theta_m)$$

$$+\text{P.V.}\int_0^{2\pi}\frac{jk}{4}\frac{F(\theta_m)-F(\theta')\cos(\theta_m-\theta')}{r_0(\theta_m,\theta')}H_1^{(2)}(kr_0(\theta_m,\theta'))\sin(n\theta_m)J(\theta')\,d\theta'$$

$$+\text{P.V.}\int_0^{2\pi}\frac{jk}{4}\frac{F(\theta')-F(\theta_m)\cos(\theta_m-\theta')}{r_0(\theta_m,\theta')}H_1^{(2)}(kr_0(\theta_m,\theta'))\sin(n\theta')J(\theta')\,d\theta'$$

$$+j\sqrt{\frac{j}{\omega\mu_0\sigma}}\frac{J(\theta_m)}{\left(\sqrt{F^2(\theta_m)+F'^2(\theta_m)}\right)^3}[F(\theta_m)\sin(n\theta_m)+F'(\theta_m)n\cos(n\theta_m)]$$

$$H_m = \frac{j}{2}\sqrt{\frac{j}{\omega\mu_0\sigma}}\,\frac{1}{\sigma}\,\frac{J(\theta_m)}{\sqrt{F^2(\theta_m)+F'^2(\theta_m)}}$$

$$U_{mn} = -\left[\int_{\Delta C_n}\frac{j}{4}H_0^{(2)}(kr_0(\theta_m,\theta'))\,d\theta' + j\sqrt{\frac{j}{\omega\mu_0\sigma}}\,\frac{\delta_{mn}}{\sqrt{F^2(\theta_m)+F'^2(\theta_m)}}\right]$$

$$C_{mn} = \int_0^{2\pi}\frac{-jk}{4}\,\frac{F(\theta')-(x_m\cos\theta'+y_m\sin\theta')}{\sqrt{(x_m-F(\theta')\cos(\theta'))^2+(y_m-F(\theta')\sin(\theta'))^2}}$$

$$\cdot H_1^{(2)}\left(k\sqrt{(x_m-F(\theta')\cos(\theta'))^2+(y_m-F(\theta')\sin(\theta'))^2}\right)\cos(n\theta')J(\theta')\,d\theta'$$

$$C'_{mn} = \int_0^{2\pi}\frac{-jk}{4}\,\frac{F(\theta')-(x_m\cos\theta'+y_m\sin\theta')}{\sqrt{(x_m-F(\theta')\cos(\theta'))^2+(y_m-F(\theta')\sin(\theta'))^2}}$$

$$\cdot H_1^{(2)}\left(k\sqrt{(x_m-F(\theta')\cos(\theta'))^2+(y_m-F(\theta')\sin(\theta'))^2}\right)\sin(n\theta')J(\theta')\,d\theta'$$

$$T_{mn} = \int_{\Delta c_n}\frac{j}{4}H_0^{(2)}\left(k\sqrt{(x_m-F(\theta')\cos(\theta'))^2+(y_m-F(\theta')\sin(\theta'))^2}\right)d\theta'.$$

Here "P.V." denotes the Cauchy principal value. Indeed, the corresponding integrals have singularities of the form $1/(\theta-\theta')$ when $\theta\to\theta'$, and thus these types of integrals are evaluated as Cauchy principal values.

## References


[1] E. Wolf, "Three-dimensional structure determination of semi-transparent objects from holographic data," *Opt. Commun.*, vol. 1, pp. 153–156, 1969.

[2] A. J. Devaney, "Reconstructive tomography with diffracting wavefields," *Inverse Problems*, vol. 2, pp. 161–183, 1986.

[3] R. M. Lewis, "Physical optics inverse diffraction," *IEEE Trans. Antennas Propagat.*, vol. AP-17, pp. 308–314, 1969.

[4] C. K Chan and N. H. Farhat, "Frequency swept tomographic imaging of three dimensional perfectly conducting objects," *IEEE Trans. Antennas Propagat.*, vol. AP-29, pp. 312–319, 1981.

[5] M. M. Ney, A. M. Smith, and S. S. Stuchly, "A solution of electromagnetic imaging using pseudoinverse transformation," *IEEE Trans. Med. Imaging*, vol. MI-3, pp. 155–162, 1984.

[6] L. Chommeloux, C. Pichot, and J. C. Bolomey, "Electromagnetic modeling for microwave imaging of cylindrical buried inhomogeneities," *IEEE Trans. Microwave Theory Tech.*, vol. MTT-34, pp. 1064–1076, 1986.

[7] D. Colton and P. Monk, "A novel method for solving the inverse scattering problem for time-harmonic acoustic waves in the resonance region II," *SIAM J. Appl. Math.*, vol. 46, pp. 506–523, 1986.

[8] G. Kristensson and C. R. Vogel, "Inverse problems for acoustic waves using the penalised likelihood method," *Inverse Problems*, vol. 2, pp. 461–479, 1986.

[9] W. Tobocman, "Inverse acoustic wave scattering in two dimensions from impenetrable targets," *Inverse Problems*, vol. 5, pp. 1131–1144, 1989.

[10] C. C. Chiu and Y. W. Kiang, "Inverse scattering of a buried conducting cylinder," *Inverse Problems*, vol. 7, pp. 187–202, 1991.

[11] M. M. Ney, "Method of moments as applied to electromagnetic problem," *IEEE Trans. Microwave Theory Tech.*, vol. MTT-33, pp. 972–980, 1985.

[12] F. M. Tesche, "On the inclusion of loss in time domain solutions of electromagnetic interaction problems," *IEEE Trans. Electromagn. Compat.*, vol. 32, pp. 1–4, 1990.

[13] E. C. Jordan and K. G. Balmain, *Electromagnetic Waves and Radiating Systems*. Englewood Cliffs, NJ: Prentice-Hall, 1968.

[14] R. F. Harrington, *Field Computation by Moment Methods*. New York: MacMillan, 1968.


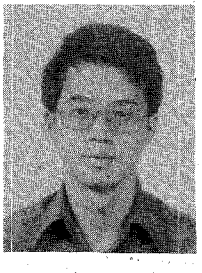


**Chien-Ching Chiu** was born in Taoyuan, Taiwan, Republic of China, on January 23, 1963. He received the B.S. degree in communication engineering from National Chiao Tung University, Hsinchu, Taiwan, in 1985 and the M.S.E.E. degree from National Taiwan University, Taipei, Taiwan, in 1987. From 1987 to 1989, he served in the R.O.C. Army Force as a communication officer. Since 1989 he has been working toward the Ph.D. degree at National Taiwan University. His current research interests include inverse scattering problems and numerical techniques in electromagnetics.


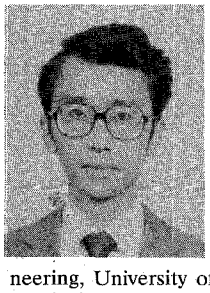


**Yean-Woei Kiang** (S'81–M'84) was born in Panchiao, Taiwan, Republic of China, on October 27, 1954. He received the B.S.E.E., M.S.E.E., and Ph.D. degrees in 1977, 1979, and 1984, respectively, all from National Taiwan University, Taipei, Taiwan, R.O.C.

In 1979 he joined the faculty of the Department of Electrical Engineering, National Taiwan University, where he is now an Associate Professor. From 1982 to 1984, he was a Visiting Scholar in the Department of Electrical Engineering, University of Illinois, Urbana-Champaign. His research interests include wave propagation, scattering, inverse scattering, and target discrimination.